

Interplay of index contrast with periodicity in polymer photonic crystals

Chris E. Finlayson,^{1,a)} Andrew I. Haines,¹ David R. E. Snoswell,¹ Andreas Kontogeorgos,¹ Silvia Vignolini,¹ Jeremy J. Baumberg,^{1,b)} Peter Spahn,² and G. Peter Hellmann²

¹NanoPhotonics Centre, Cavendish Laboratory, University of Cambridge, Cambridge CB3 0HE, United Kingdom

²Deutsches Kunststoff-Institut (DKI), Schlossgartenstrasse 6, D-64289 Darmstadt, Germany

(Received 26 July 2011; accepted 2 December 2011; published online 30 December 2011)

We report how the strength of resonant Bragg reflection from polymeric photonic crystals (polymer opals) varies linearly with the refractive-index contrast, Δn , in contrast to the quadratic buildup of Fresnel reflections scaling as $(\Delta n)^2$. This occurs due to the interplay of disorder and periodicity, in agreement with a simple 1-dimensional periodic model. Goniometry experiments show that opal films exhibit “cones” of resonantly scattered light, which extend to $\pm 20^\circ$ angular deviation from the specular direction. The intensity of the scattering cones varies super-linearly with Δn . Such medium contrast photonic crystals are of significant interest for understanding structural colors exhibited in nature, by structures with inherent disorder. © 2011 American Institute of Physics. [doi:10.1063/1.3672215]

An industrial-scale technique to produce flexible photonic crystals has recently been developed using shear-ordering of sub-micron-sized core/shell polymer particles.^{1,2} This produces flexible polymer cubic-lattice opaline films, with fundamental optical resonances tunable across the visible and near-infrared regions (by varying the precursor nanoparticle size from 200 to 350 nm, and hence the resulting lattice parameter). Such polymeric opals have intrinsic advantages over other self-assembling colloidal systems,^{3,4} in which the structures formed are solvent-free and permanently formed into a visco-elastic solid.⁵ The refractive index contrast between the core beads and the matrix polymer is essential for the appearance of such structural color, through spectrally resonant multiple Bragg scattering.⁶ However, it is not clear how the strength of such resonances changes as the index contrast increases. Besides the technological applications, such systems are interesting analogues of structural color in nature (such as butterflies or beetles^{7,8}), as well as the intensity of scatter from clouds and radar imaging.

In this paper, we study the effect of the refractive index contrast, Δn , on the resonant scattering and reflectivity of polymer photonic crystals, within a regime of $\Delta n < 0.2$. In earlier work, we reported the synthesis of core/shell (CS) structures based on rigid cross-linked polystyrene (PS) spheres, capped by a soft poly-ethylacrylate (PEA) shell, as illustrated in Figure 1(a).^{1,9} The refractive index contrast between core and shell materials can be varied by controlling the chemical composition of the shell material using low refractive-index fluorinated monomers. Here, we study samples with $\Delta n = 0.05$ – 0.18 and with CS particle diameters of 250–300 nm, giving Bragg resonances in the red (Table I). Opaline films of thickness $\sim 100 \mu\text{m}$, with highly uniform ordering, are produced using a combination of linear- and edge-shearing of the as-synthesized batches of the CS mate-

rial, as previously reported.¹⁰ A small amount (0.05% by weight) of an absorbing carbon-nanoparticle powder is also pre-mixed into the opals by extrusion, significantly increasing the color saturation of the opals without disrupting the lattice quality.^{6,10}

The calibrated normal incidence reflectivity of samples is measured with an adapted microscope, using a focal spot diameter of $\sim 2 \mu\text{m}$ ($\times 20$ magnification) and collection via suitable focusing optics and a fiber-coupled CCD spectrometer. The bright-field reflectance spectra of samples 1-5 (Fig. 2(a)) show intensity increasing with Δn ; Figure 2(c) shows a clear linear relationship. The small (non-systematic) shifts in Bragg wavelength are due to slight fluctuations in the mean CS diameters and in the average refractive index (n_{av}). However, the strength of each individual scattering is given by the Fresnel reflectivity (for uniform interfaces) or Mie scattering (for particles), both proportional to $(\Delta n/n_{av})^2$,¹¹ as also found in periodic structures.¹²

To explain these observations, we have developed a 1D multilayer quasi-model of the opaline structures.⁵

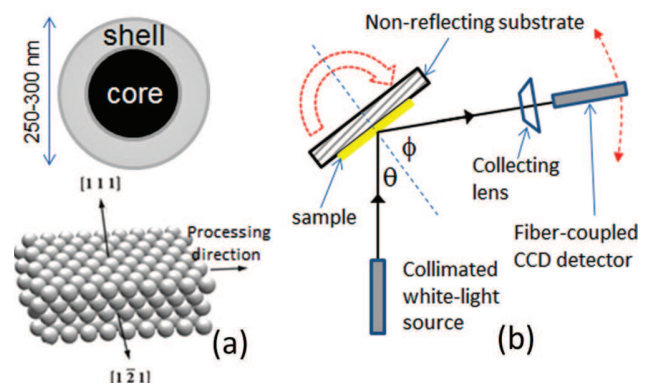


FIG. 1. (Color online) (a) Core/shell architecture of precursor particles (top), self-assembled into polymer opals (below). The relative orientations of the [111] lattice plane and the shear-processing direction are shown. (b) Schematic of experimental goniometer, with angles of incidence (θ) and detection (ϕ) relative to sample normal as indicated.

^{a)}Electronic mail: cef2@aber.ac.uk. Present address: Institute of Mathematical & Physical Sciences, Prifysgol Aberystwyth University, Wales SY23 3BZ, United Kingdom.

^{b)}Electronic mail: jjb12@cam.ac.uk.

TABLE I. Characteristic parameters of samples; average refractive-index (n_{av}) from refractometry, calculated Δn , mean particle size from hydrodynamic chromatography, and measured normal incidence Bragg wavelength (λ_{111}). See Ref. 9 for further details.

Sample	n_{av}	Δn	CS size (nm)	λ_{111} (nm)
1	1.488	0.18	270	595
2	1.505	0.15	285	580
3	1.517	0.12	280	605
4	1.548	0.07	275	625
5	1.565	0.05	255	680

Representing the periodicity of the opals, rather than their exact dimensions, this consists of $\lambda/4$ layer-pair stacks of the high and low n components giving resonance at $\lambda = 600$ nm, with absorbance (α) due to the measured effect of the carbon dopant. In addition, the layers have a Gaussian-distributed thickness error of width γ , which accounts for deviations from perfect crystalline order within the photonic crystal. The reflectivity spectra of these model structures were calculated using a transfer-matrix method averaged over many cycles,¹³ with 100 layer-pairs (roughly corresponding to a sample of thickness several 10s of microns), using suitable parameters. Representative results are shown in Figure 2(b), with a value of $\gamma = 15$ nm (or 7% of layer thickness variation) yielding peak reflectances in close agreement with experiment for each Δn value studied and also giving realistic spectral FWHM values of 50–60 nm. As discussed previously, such a model results in Lorentzian spectral profiles.⁵ The linear dependence of the predicted peak intensities on Δn is shown in Figure 2(c), with excellent agreement to the experimentally observed trend. The predicted quadratic dependency from Fresnel theory is modified by disorder in such opals, to produce a linear dependence on $|\Delta n|$. Coherent superposition at the reflectance peak is disrupted by the cumulative phase shifts from thickness fluctuations (disorder) since the light penetrates to depths of hundreds of layers in such low Δn systems. We expect this to be important in the regime where $(n_{av}\gamma)/(\Delta nL) > \pi$, where L is the sample thickness. This is because both the Bragg length, of order $L_B = \lambda\Delta n/n_{av}$, and the mean free path are smaller than the ordered opal thickness for all of the Δn values under study.^{14,15} Hence, the degree of disorder in the sample demonstrably plays a fundamental role in these linear dependencies. In previous studies of polymer opals, we presented crystallographic evidence of stacking faults and/or twinning within the cubic structures, which introduces a certain level of disorder throughout the films.^{10,16} It is likely that these characteristics are also *intrinsic* to many self-assembled periodic structures, including those found in nature.^{17,18}

In order to study the resonantly scattered light at non-specular angles (the so-called “scattering cone” (Ref. 14)), samples are measured using goniometry (Figure 1(b)). Samples are illuminated using a thermal white-light source, collimated to a spot size of a few mm, and reflected light is detected via a collecting lens (solid-angle of collection $\sim 10^{-7}$ sr) and fiber-coupled spectrometer. Careful alignment allowed both the detector and the sample stage to be rotated about a common axis, co-centred on the point where the light source is incident on the sample. The angular deviation (δ),

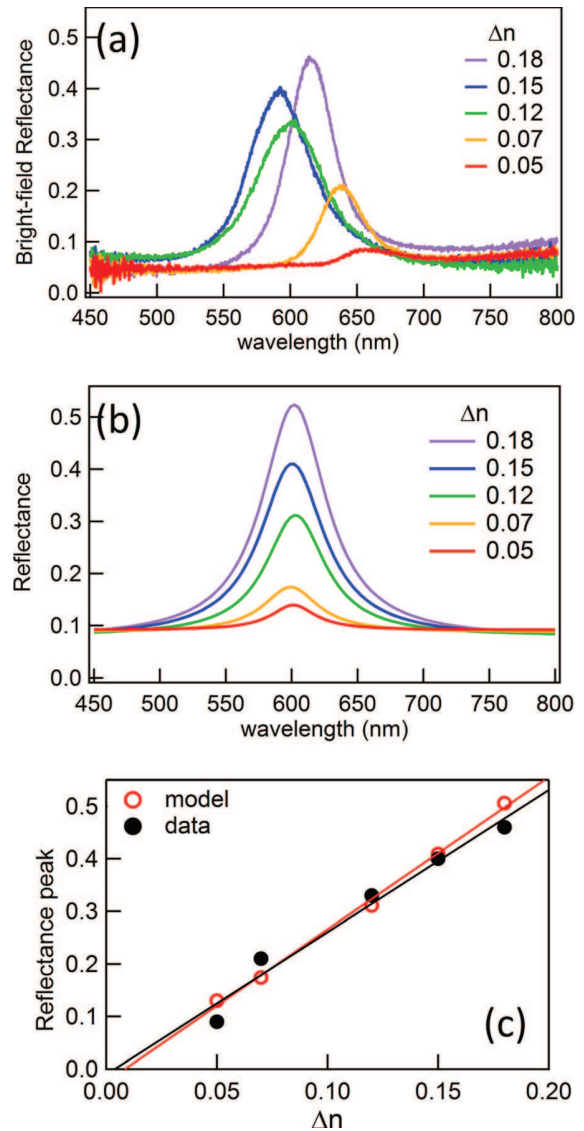


FIG. 2. (Color online) (a) Normal incidence bright-field reflectance spectra for a series of red opal films with increasing refractive index contrast. These samples were doped with 0.05 wt. % of carbon. (b) Reflectance spectra based on a corresponding 1D multilayer model, with parameters $\lambda_{\text{peak}} = 600$ nm, 100 layer-pairs, $\gamma = 15$ nm and $\alpha = 8.9 \times 10^3 \text{ m}^{-1}$. (c) Reflectance peak heights plotted vs. index contrast, Δn , with linear fits.

relative to the specular reflection at $-\theta$ is thus given by the relation $\delta = \phi - \theta$, where θ and ϕ are the angles of incidence and detection respectively. By normalizing the detected light to the specular reflection from a reflective aluminum mirror, optical spectra of the scattered light as a function of δ are extracted, allowing comparison between samples with different Δn . The raw data (Fig. 3(a)) shows wide scattering cones around the specular reflection, with the resonantly scattered light shifting across the λ_{111} peak, from short to long wavelengths, as δ increases. By considering the change in wavevectors involved ($\Delta \mathbf{k}$), the data can be exactly transformed into reciprocal $\Delta \mathbf{k}$ -space (assuming low index contrast) using

$$\begin{aligned} \Delta \mathbf{k} &= (\Delta k_x, 0, \Delta k_z) \\ &= n_{av} k_0 (\sin \theta'_{out} - \sin \theta'_{in}, 0, \cos \theta'_{out} - \cos \theta'_{in}), \end{aligned} \quad (1)$$

with the optical wavevector magnitude, $|k_0| = 2\pi/\lambda$ and θ'_{in} , θ'_{out} the angles of incidence and scattering *inside* the sample. The shape of the \mathbf{g}_{111} reciprocal lattice point (Figure 3(b)) reveals the disorder in both layer spacing (Δk_z) and lateral fluctuations (Δk_x) responsible for the scattering cones. As Δn increases from 0.05 to 0.18, the intensity of the scattering cone increases commensurately, while the effect on the

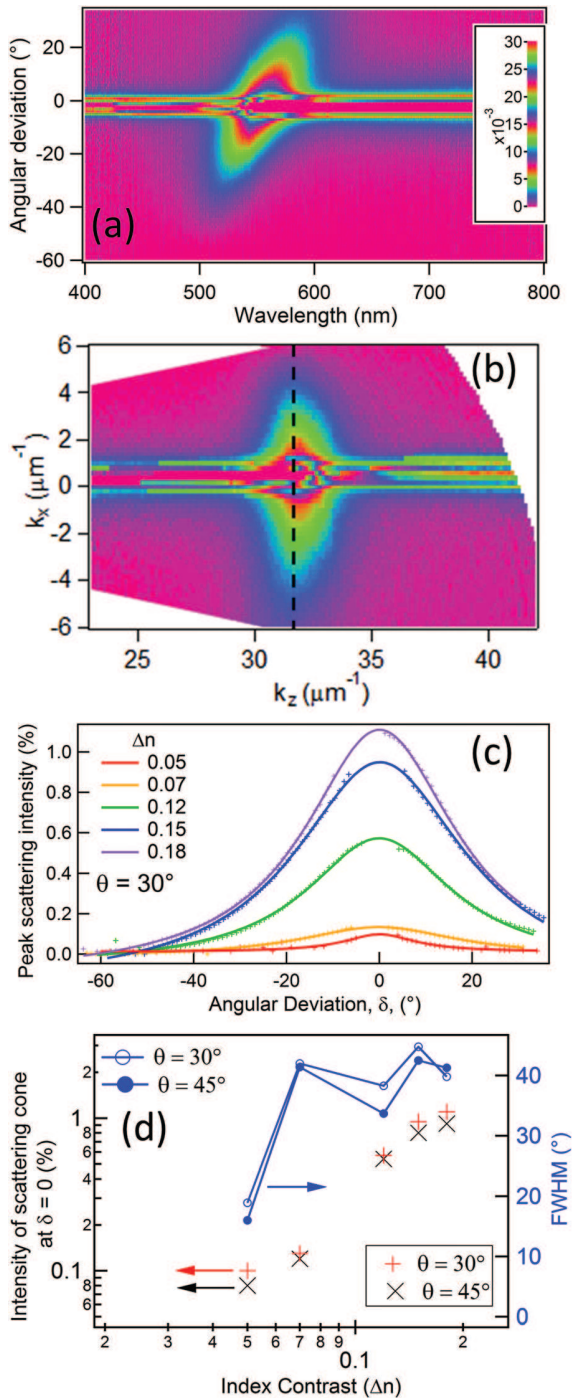


FIG. 3. (Color online) (a) Scattered light spectra for representative $\Delta n = 0.15$ sample, (b) transformed into k -space as projected onto the k_z - k_x plane. The reciprocal lattice vector \mathbf{g}_{111} is at $k_z = 32 \mu\text{m}^{-1}$. (c) Peak scattering intensity as a function of angular deviation, δ , relative to the specular-reflection direction ($-\theta$). (d) Maximum scattering intensity and FWHM of scattering cones for $\theta = 30^\circ$ and 45° . For clarity, the index contrast is displayed on a logarithmic axis.

angular width of the cone is weak. Fitting cross-sections of k_x gives lateral broadenings with FWHM $\sim 3 \mu\text{m}^{-1}$, corresponding to real-space dimensions of $3\text{--}5 \mu\text{m}$, and implying that there are lateral defects of size around 10 times the crystal layer spacing. This result hence gives a first order indication of the presence of lateral fluctuations in the alignment of parallel chains in each layer within these photonic crystals.

Extracting the peak spectral scattering intensity as a function of δ (Figure 3(c)) for each sample results in Lorentzian angular scattering profiles, as consistent with both the above analysis and earlier studies, which implied that defects spatially localize light over length scales of many sphere periods.⁶ Note that peak scattering values were extracted by following the locus of the \mathbf{g}_{111} reciprocal lattice point, as shown by the dashed line in Figure 3(b). The scattering strength increases super-linearly as a function of Δn within this low index-contrast regime (Fig. 3(d)) and this result is replicated when measuring with different angles of incidence (θ). The angular width of the scattering cones of all samples extends to $\pm 20^\circ$ from the specular direction (Fig. 3(d)), with the exception of the lowest index-contrast sample. These observations contrast with those on high Δn opals, which exhibit an additional isotropic surface scattering that leads to spectral dips,¹⁵ rather than the scattering peaks we always observe. Further theoretical and experimental investigation is required to fully explain the origin of this cone width, which is related to the lateral scale length of disorder in the samples. We note that all samples are mounted identically, with the shear processing direction in the same plane as source and detector, removing effects of anisotropy due to the orientation of the [111] lattice planes (see also Figure 1(a)).¹⁹

In conclusion, we demonstrate how the light scattered from polymeric photonic crystals depends on the refractive-index contrast. In this lower refractive-index contrast regime, the resonant Bragg reflection intensity varies linearly with Δn , in good agreement with a transfer-matrix model which incorporates the effects of disorder. Such polymer opal systems are of interest as exemplars of self-assembled periodic structures found in nature. Goniometry reveals cones of resonantly scattered light, which extend to $\pm 20^\circ$ angular deviation from the specular direction, whose intensity depends super-linearly on Δn . A full understanding of the interplay of disorder and index contrast in the low Δn regime thus requires revised theoretical models.

This work was supported by EPSRC (UK) grants EP/G060649/1 and EP/E040241.

¹T. Ruhl, P. Spahn, and G. P. Hellmann, *Polymer* **44**, 7625 (2003).

²O. L. J. Pursiainen, J. J. Baumberg, H. Winkler, B. Viel, and T. Ruhl, *Appl. Phys. Lett.* **87**, 101902 (2005).

³Y. Xia, B. Gates, and Z.-Y. Li, *Adv. Mater.* **13**, 409 (2001).

⁴R. de la Rue, *Nature Mater.* **2**, 74 (2003).

⁵D. R. E. Snoswell, A. Kontogeorgos, J. J. Baumberg, T. D. Lord, M. R. Mackley, P. Spahn, and G. P. Hellmann, *Phys. Rev. E* **81**, 020401 (2010).

⁶O. L. J. Pursiainen, J. J. Baumberg, H. Winkler, B. Viel, P. Spahn, and T. Ruhl, *Opt. Express* **15**, 9552 (2007).

⁷P. Vukusic and J. R. Sambles, *Nature* **424**, 852 (2003).

⁸P. Simonis and J. P. Vigneron, *Phys. Rev. E* **83**, 011908 (2011).

⁹P. Spahn, C. E. Finlayson, W. Mbi Etah, D. R. E. Snoswell, J. J. Baumberg, and G. P. Hellmann, *J. Mater. Chem.* **21**, 8893 (2011).

¹⁰C. E. Finlayson, P. Spahn, D. R. E. Snoswell, G. Yates, A. Kontogeorgos, A. I. Haines, G. P. Hellmann, and J. J. Baumberg, *Adv. Mater.* **23**, 1540 (2011).

- ¹¹E. Hecht, *Optics*, 2nd ed. (Addison Wesley, Boston MA, 1987).
- ¹²S. Satpathy, Ze Zhang, and M. R. Salehpour, *Phys. Rev. Lett.* **64**, 1239 (1990).
- ¹³M. Born and E. Wolf, *Principles of Optics: Electromagnetic Theory of Propagation, Interference and Diffraction of Light* (Pergamon, Oxford, UK, 1964).
- ¹⁴J. J. Baumberg, O. L. Pursiainen, and P. Spahn, *Phys. Rev. B* **80**, 201103 (2009).
- ¹⁵S. G. Romanov, *J. Appl. Phys.* **103**, 093117 (2008).
- ¹⁶O. L. J. Pursiainen, J. J. Baumberg, H. Winkler, B. Viel, P. Spahn, and T. Ruhl, *Adv. Mater.* **20**, 1484 (2008).
- ¹⁷Y. A. Vlasov, V. N. Astratov, A. V. Baryshev, A. A. Kaplyanskii, O. Z. Karimov, and M. F. Limonov, *Phys. Rev. E* **61**, 5784 (2000).
- ¹⁸Z. L. Wang, C. T. Chan, W. Y. Zhang, Z. Chen, N. B. Ming, and P. Sheng, *Phys. Rev. E* **67**, 016612 (2003).
- ¹⁹A. Kontogeorgos, D. R. E. Snoswell, C. E. Finlayson, J. J. Baumberg, P. Spahn, and G. P. Hellmann, *Phys. Rev. Lett.* **105**, 233909 (2010).